Received: 18 July 2025 | Revised: 27 January 2026 | Accepted: 30 January 2026

DOI: 10.1002/qj.70147

Quarterly Journal of the Royal Meteorological Society RMetS

RESEARCH ARTICLE

Simulating the year to minute wind spectrum with mesoscale-coupled large-eddy simulations

Bernard Postema[1,2] | **Chiel C. van Heerwaarden**[2] | **Bart J.H. van Stratum**[2] | **Pim van Dorp**[1] | **Peter Baas**[1] | **Harm J.J. Jonker**[1,3]

[1]Whiffle B.V., Delft, the Netherlands

[2]Meteorology and Air Quality Group, Wageningen University & Research, Wageningen, the Netherlands

[3]Department of Geoscience and Remote Sensing, Delft University of Technology, Delft, the Netherlands

Correspondence
Bernard Postema, Whiffle B.V., Molengraaffsingel 8, 2629 JD, Delft, the Netherlands.
Email: bernard.postema@whiffle.nl

Abstract

By coupling large-eddy simulation (LES) codes to weather data from large-scale models, previous studies showed the viability of "real-weather" LES. However, when simulating extended periods (up to one year) of weather, a number of them diagnosed an underestimation of the simulated temporal spectrum (of wind and solar irradiance) at timescales of a few hours (i.e., the atmospheric mesoscale). This study presents simulations aimed at reproducing the observed wind spectrum from timescales of one year to one minute, including the mesoscale. Reanalysis data (European Centre for Medium-Range Weather Forecasts Reanalysis Version 5) are used as boundary conditions to a mesoscale simulation with either a local or a non-local formulation of vertical diffusion, which then drives an LES (resolution of 50 m). Several domain sizes are used to simulate the weather during 2022 over a meteorological tower in The Netherlands. It is shown that, when increasing the size of the mesoscale simulation from 64 km to 1024 km, the LES wind spectrum at the mesoscale approaches the observed spectrum. The spectrum is also sensitive to the mesoscale diffusion formulation, which either resolves or suppresses explicit convection, resulting in a different LES wind spectrum. In addition, it is shown that the higher order statistics (structure functions) improve by using a large enough mesoscale simulation. The results indicate that LES can be used as a tool to simulate the temporal dynamics of the wind at all timescales between one minute and one year, if the atmospheric mesoscales are taken into account appropriately.

KEYWORDS

atmospheric turbulence, large-eddy simulation, mesoscale meteorology

1 | INTRODUCTION

Atmospheric models use discretized physical laws and approximations to simulate a part of the wide spectrum of motions in the atmosphere, which spans from synoptic systems down to turbulence dissipation. The model's domain size sets the upper limit on the scales that it can resolve and is bounded by the size of the Earth, and the lower limit is set by the model's resolution. Progress in atmospheric modeling is often not measured by breakthroughs in the model physics, but rather by an increase in domain size, resolution, integration time, or ensemble size, because those factors improve the practical usability of the model output (Bauer *et al.*, 2015).

One area where weather modeling is progressing to finer resolutions, longer integration times, and larger domains is atmospheric large-eddy simulations (LES). When coupled to weather data from external models, such models can be described as "real-weather LES", because they use realistic inflow conditions. Real-weather LES can be used to study turbulent flow, small clouds, land–atmosphere interactions, renewable energy applications, and so on (e.g. Arthur *et al.*, 2020; Baas *et al.*, 2023; Haupt *et al.*, 2019; Heinze *et al.*, 2017; Schemann *et al.*, 2020; Talbot *et al.*, 2012). Because of its increased realism and practical usability, real-weather LES can contribute to addressing the so-called "hectometric modeling challenge" (Lean *et al.*, 2024).

By coupling an LES with periodic boundary conditions to a regional weather model and running one full year of weather conditions on a domain of 25 km by 25 km, Schalkwijk *et al.* (2015a) showed the viability of real-weather LES over a range of timescales and weather conditions. When considering the energy spectrum of the horizontal wind speed, however, they diagnosed an underestimation of wind-speed variance at temporal scales between roughly one and 10 hours. This points to a lack of variability in the atmospheric mesoscale, and therefore an incorrect representation of the cascade of motion from large-scale weather to the turbulent scale. In a more recent study, Stratum *et al.* (2023) found a similar variance deficit in radiation as simulated by a periodic LES in a real-weather setting. Schalkwijk *et al.* (2015a) hypothesized that using larger domain sizes of about 200 km would permit mesoscale phenomena and thereby resolve the missing variance in the spectrum.

To explore this hypothesis, we present real-weather LES simulations with open boundary conditions, which are coupled to global weather data—the European Centre for Medium-Range Weather Forecasts (ECMWF) Reanalysis Version 5 (ERA5)—in a nested approach, via a coarser mesoscale simulation with domain sizes of $\mathcal{O}(100\,\text{km})$ and horizontal resolution of 2 km. Both local- and non-local formulations of vertical diffusion will be used for the mesoscale simulation, which represents two contrasting ways of dealing with the problem of the gray zone of atmospheric convection (Honnert *et al.*, 2020). The purpose of the study is therefore to show how adding mesoscale structures to the LES inflow affects the statistical metrics of the LES wind across timescales. The energy spectrum will be the main method of analysis, but also the wind increments and structure functions will be considered. These latter two quantify the higher order statistics of the flow, which are not represented by the energy spectrum but are very pronounced in turbulent flow.

The current study takes the LES as a starting point and progressively introduces larger atmospheric scales to represent mesoscale effects. Other models that were originally developed as LES codes and are moving to increasing realism are described by Maronga *et al.* (2020), Sauer and Muñoz-Esparza (2020), Heerwaarden *et al.* (2017). On the other hand, it is also possible to develop real-weather LES by starting with a mesoscale model and adding microscale nests. Such efforts are described in, for example, Talbot *et al.* (2012) and Heinze *et al.* (2017). Other works describing and testing coupled mesoscale to microscale simulations include Haupt *et al.* (2019), who summarize mesoscale to microscale coupling strategies specifically aimed at wind-energy application, and Rai *et al.* (2019), who studied the impact of resolution and turbulence parametrizations in such model configurations.

Most research using these models uses limited simulation periods (days), and therefore does not discuss the representation of the full range of atmospheric motion (seasons to minutes) in the simulations. Recently, however, Peña and Mirocha (2024) performed a year-long multiscale simulation of a site in Denmark and compared model output with wind observations in a nested setup similar to the one used here. In line with Schalkwijk's hypothesis, they do not find a spectral gap underestimating the energy at mesoscales. These considerations combined motivate a dedicated study of the representation of the atmospheric mesoscale in LES.

This article is structured as follows. Section 2 gives theoretical background on spectral analysis, wind increments, and structure functions applied to atmospheric flow. Then, the employed LES code and observation data are presented in Section 3. The results and discussion (Section 4) first aim to identify the key sensitivities in the wind spectrum during one month (Section 4.1). Then simulations of the full year of 2022 are analyzed in terms of the energy spectrum, wind increments, and structure functions (Section 4.2). Finally, before drawing conclusions in Section 5, a meteorological interpretation of the results is given in Section 4.3.

2 | BACKGROUND

2.1 | Spectral analysis of atmospheric flow

Kolmogorov (1941) postulated that, under the assumptions of local homogeneity and local isotropy, the statistics of turbulent flow at each length scale depend only on the total energy dissipation rate and the length scale (Frisch, 1995, p. 75). This concept can be used to show that, on dimensional grounds, the energy is distributed across spatial scales according to the $-5/3$ law:

$$E(k) = C\epsilon^{-2/3}k^{-5/3}, \tag{1}$$

where $E(k)$ is the energy per wavenumber per unit mass, k is the wavenumber (with dimension inverse length), C is a dimensionless constant, and ϵ is the energy dissipation (with dimension energy per unit mass per unit time). Using Taylor's hypothesis of frozen turbulence, the spatial wavenumber k can be converted to a temporal frequency ω, which means that the temporal spectrum $E(\omega)$ is equivalent to the spatial spectrum and therefore also proportional to $\omega^{-5/3}$. The length of the simulated period in real-weather LES (up to one year) is much larger than the spatial scales that correspond to such periods. Therefore, the temporal spectrum (rather than the spatial one) is most suited to studying how large-scale phenomena propagate into the LES. Also, in observations, it is more feasible to obtain wind data with a large temporal extent than data with a large spatial extent. Hence, we will consider temporal spectra in this study. To calculate the total energy spectrum of the horizontal wind, both components of the horizontal wind are needed. In this study, however, we limit the analyses to spectra of the magnitude of the horizontal wind, because the observation data are obtained with a cup anemometer. This is an instrument that measures the magnitude of the horizontal wind, and calculating the separate components by using the wind direction introduces an unnecessary error. Specifically, we consider the Fourier transform, denoted with a hat, of the magnitude of the horizontal wind $M(t)$. Then the energy spectrum is calculated by squaring the magnitude of the Fourier-transformed wind:

$$E_M(\omega) = |\hat{M}(\omega)|^2. \tag{2}$$

By integrating this energy spectrum, one can retrieve the variance of $M(t)$. In this study, the term variance is therefore not limited to the below-hour (or three-dimensional) fluctuations in the wind (like it is in some meteorological texts), but can refer to variations at any timescale. To account for the logarithmic horizontal axis, spectra are plotted as $\omega \cdot T \cdot E_M(\omega)$ (where T is the length of the time series), which makes the Kolmogorov spectrum proportional to $\omega^{-2/3}$, and averaged over logarithmically spaced frequency bins to reduce noise.

Panofsky and van der Hoven (1955) and der Hoven (1957) identified a minimum in the spectral energy of the near-surface horizontal wind, located between approximately several hours and 10 minutes. Such a spectral gap justifies the separation of atmospheric flow into slow- and fast-varying components (the premise of Reynolds decomposition), and was speculated to have implications for atmospheric predictability too (Lorenz, 1969). The existence (and/or visibility) of the spectral gap has been debated (Lilley *et al.*, 2008; Schertzer & Lovejoy, 2004). For example, Larsén *et al.* (2016) find that, depending on the contributions of mesoscale and microscale variance, a spectral gap can appear in the near-surface winds but becomes invisible at larger heights. From airplane campaigns, Nastrom and Gage (1983, 1985) and Nastrom *et al.* (1984) showed that spatial wind spectra show a $-5/3$ spectrum extending from a few to a several hundred kilometers. The physical mechanism responsible for this observation has been a topic of theoretical debate (Lindborg, 1999), observational studies (Callies *et al.*, 2014), and modeling studies, using both global models (Tung & Orlando, 2003) and LES (De Roode *et al.*, 2004). In the current study, we will not study the physical origin of the shape of the spectrum of atmospheric flow, but instead use it as a tool to judge the quality of the simulations.

2.2 | Velocity increments, wind ramps, and structure functions

Kolmogorov (1941) introduced the assumptions that lead to the $-5/3$ spectrum, but he did not use spectral analysis. Instead, he used an equivalent metric, based on the second-order statistics of the velocity increments over varying distances in the fluid. Here, in line with using the temporal spectrum, we use the temporal velocity increments, at varying lag times τ:

$$\delta_M(t,\tau) = M(t) - M(t-\tau), \tag{3}$$

which can be interpreted as so-called "wind ramps", that is, the increase or decrease of wind between times $t-\tau$ and t. These wind ramps have a strong influence on wind-energy production and are relevant at various timescales, ranging from the mesoscale to the day-scale (Cheneka *et al.*, 2020). Distributions of $\delta_M(t,\tau)$ at a fixed τ (for example 10 minutes) are very non-Gaussian, with a heavy tail (DeMarco & Basu, 2018; Sim *et al.*, 2024).

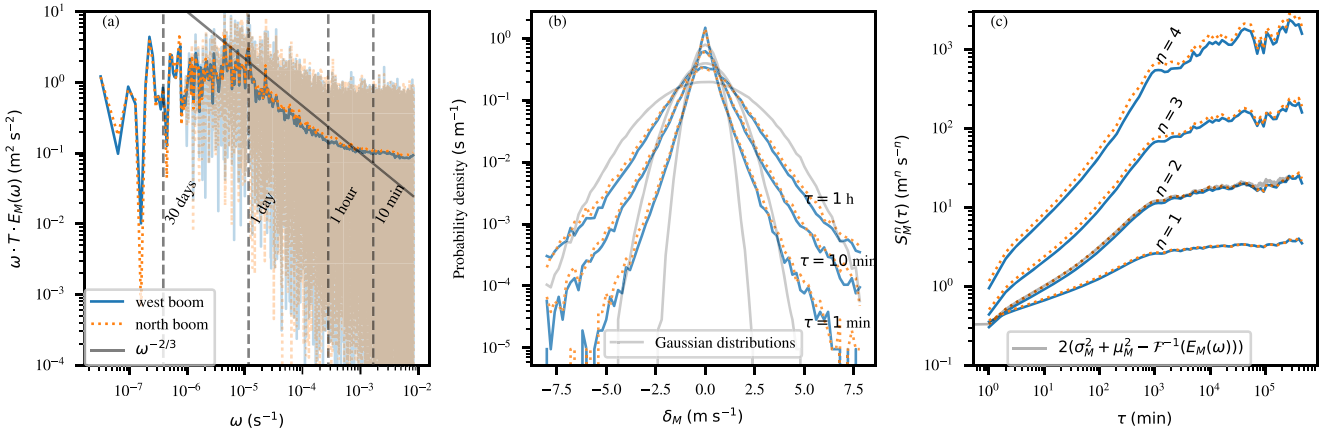

FIGURE 1 An overview of the concepts used in this study, applied to one year of one-minute cup anemometer data (at 80-m height) at the Cabauw tall tower, the Netherlands (see Section 3 for more details). (a) Energy spectra of the wind, including the same spectra averaged over logarithmically increasing bins. (b) Probability densities of the wind increments at lag times of 1 minute, 10 minutes, and 1 hour, with a logarithmic vertical axis, including several Gaussian distributions. (c) Structure functions for $n = 1, 2, 3, 4$, also including an evaluation of Equation (5).

Taking the nth-order moment of the absolute value of the velocity increments gives the so-called nth *structure function* of $M(t)$:

$$S_M^n(\tau) = \overline{|\delta_M(t,\tau)|^n}, \tag{4}$$

where the overbar denotes an average over t. The structure functions for $n = 1, 2, 3, 4, \ldots$ quantify the different moments of the velocity increments as a function of lag time. They are directly related to the cumulants of the distribution, which are the mean, variance, skewness, and kurtosis, respectively.

When expanding the second structure function, the autocovariance of $M(t)$ appears, which, by the autocorrelation theorem (or Wiener–Khinchin theorem), is equal to the inverse Fourier transform of the energy spectrum of $M(t)$. It can then be shown that the second structure function is related to the energy spectrum by

$$S_M^2(\tau) = 2(\sigma_M^2 + \mu_M^2 - \mathcal{F}^{-1}[E_M(\omega)]), \tag{5}$$

where frequency and lag time are related by $\tau = \omega^{-1}$. Equation (5) shows that there is a direct mapping from the second structure function to the energy spectrum. Hence, the information in both metrics is equivalent.

The three main statistical concepts used in this study—the energy spectrum, wind increments, and structure functions—are interlinked by the characteristic dynamics of turbulent (atmospheric) flow. Figure 1 shows an overview of these concepts for one-minute wind observations.

3 | MODEL AND DATA

This section will first describe the atmospheric modeling system used in this study (Section 3.1), then the specific model settings and domain sizes that are used (Section 3.2), and finally the observation data (Section 3.3).

3.1 | ASPIRE

The Atmospheric Simulation Platform for Innovation, Research, and Education (ASPIRE) is an atmospheric modeling suite designed for real-weather LES and has its roots in the Dutch Atmospheric Large Eddy Simulation (DALES: Heus *et al.*, 2010). ASPIRE is developed at the company Whiffle, a spin-off of the Delft University of Technology, the Netherlands, and is applied mostly in the renewable energy sector. The model runs mostly on graphics processing units (GPUs: Schalkwijk *et al.*, 2012, 2015b) and, more recently, open boundary conditions and the addition of mesoscale nesting have been introduced (Storey & Rauffus, 2024). Furthermore, ASPIRE has modules for radiation, microphysics, the land surface, and wind turbines. ASPIRE has been applied for wind-farm modeling (Baas *et al.*, 2023; Oldbaum, 2019; Postema *et al.*, 2025; Verzijlbergh, 2021; Williams *et al.*, 2024), wind turbine physics and loads (Schepers *et al.*, 2021; Taschner *et al.*, 2023), wind forecasting (Alonzo *et al.*, 2022; Gilbert *et al.*, 2020), wind climate modeling (Kantharaju *et al.*, 2023; Storey & Rauffus, 2024), and dispersion (Bieringer *et al.*, 2021).

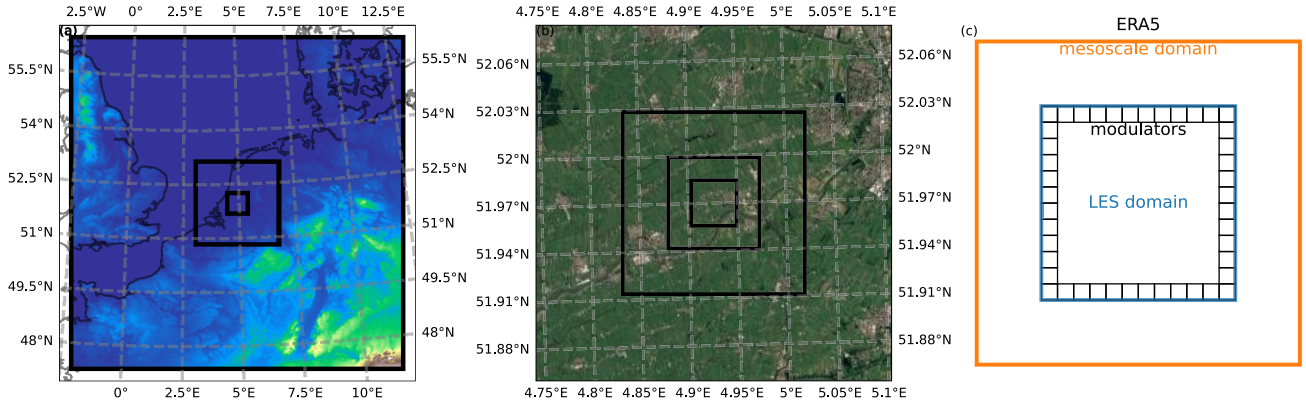

FIGURE 2 Domain setup of the simulations performed in this study. (a) Terrain map used in the simulations (shading) and the mesoscale domains (squares). (b) LES domains (squares) (satellite image from Google). (c) Schematic view of the coupling strategy, including the position of the modulators that create turbulent inflow conditions for the LES.

LES runs with ASPIRE are nested in a mesoscale-type simulation, typically with a horizontal resolution of 2 km, which has the same model formulation as the LES, except for turbulence, which is completely parametrized. This is done with a Smagorinsky-type diffusion scheme in the horizontal direction. In the vertical direction, simulations with a local diffusion scheme (Holtslag & Boville, 1993), as well as a non-local formulation (Troen & Mahrt, 1986), can be performed. The non-local scheme is only applied to temperature, and the boundary-layer height is defined as the height where the potential temperature is 1 K above its surface value. The boundary conditions (lateral and top) of the mesoscale simulation are derived from ERA5 reanalysis data (Hersbach *et al.*, 2020).

In the LES, an anisotropic minimum dissipation (AMD) turbulence parametrization is used (Abkar *et al.*, 2016; Abkar & Moin, 2017; Rozema *et al.*, 2015; Verstappen, 2011) for subgrid turbulence parametrization. AMD models are designed to apply a minimum amount of subgrid dissipation, and differ from classical eddy-viscosity type subgrid models because they do not rely on the bulk vertical shear. This characteristic makes AMD models switch off in stably stratified flows (Abkar & Moin, 2017), allowing stronger wind shear than eddy-viscosity models. AMD models do not have an internally consistent way to diagnose subgrid turbulence kinetic energy.

To generate turbulent inflow conditions in the LES, a concurrent precursor method (Stevens *et al.*, 2014) is used. In our approach, the main LES domain is surrounded by a series of identical periodic LES domains, termed "modulators" (Figure 2c). The modulators are forced with mean profiles taken from the center of the mesoscale domain and have the same resolution as the main LES. The turbulent fields generated by the modulators (i.e., differences from the mean profile) are then introduced into the main LES. In this study, the modulators have 64 by 64 horizontal grid points, so their number varies depending on the size of the main LES domain.

ASPIRE uses an Arakawa C grid (Arakawa & Lamb, 1977) for spatial discritization, with an exponentially stretched grid in the vertical direction. Timestepping is done with a third-order Runge–Kutta scheme.

Both the LES and mesoscale simulation use a modified version of the Tile ECMWF Scheme for Surface Exchanges over Land (TESSEL: ECMWF, 2017) for the land surface. Terrain data are taken from the Ensemble Digital Terrain Model (Ho *et al.*, 2023). Furthermore, ASPIRE uses the Charnock (1955) roughness parametrization over water surfaces, ESA worldcover data for land use (Zanaga *et al.*, 2022), the ECMWF radiation scheme ecRAD (Hogan & Bozzo, 2018), and microphysics according to Grabowski (1998) and Khairoutdinov and Randall (2003). Orography is represented by an immersed boundary method (IBM) similar to that in Suter *et al.* (2022), with the solid-fluid boundary defined at the cell faces and the subgrid-scale stresses adapted to the presence of the surface following Monin–Obhukov similarity theory. With a vertical spacing of 25 m in the LES, situations can occur when similarity theory might not be valid, because it is applied outside the surface layer, which can be shallow in stable stratifications. Optis *et al.* (2016) studied the limitations of similarity theory at the Cabauw site for those reasons. Their results suggest that, below roughly 50 m in stable stratifications, the wind profiles obtained by similarity theory still match observed profiles reasonably well. It is therefore expected that the vertical resolution used in this study is sufficient to justify the use of similarity theory in stable stratifications.

TABLE 1 The domain configurations of the mesoscale simulations and LES presented in this study, and the corresponding horizontal resolution (d_x), vertical resolution at the surface (d_z), horizontal domain size (L), vertical domain size (L_z), and simulation period.

	d_x (m)	d_z (m)	L (km)	L_z (m)	Period
Mesoscale simulation (parent)	2000	40	64	8000	2022
			256		
			1024		
LES (child)	50	25	3.2	3000	April 2022
			6.4		April 2022
			12.8		2022

3.2 | Setup of the simulations

The specific simulation setups used in the current study are described below; see also Figure 2 and Table 1. In all cases, a one-way nested simulation is employed, in which one LES is child to one parent mesoscale simulation, which is driven by ERA5 boundary conditions. The horizontal dimensions of the domains, however, are varied. LES runs with three different horizontal sizes are presented: 3.2, 6.4, and 12.8 km. The horizontal size of the mesoscale simulation is varied between 64, 256, and 1024 km. Because each mesoscale simulation is parent to three LES domains, this results in nine different domain configurations. Each of these setups is run with a local formulation of vertical diffusion and a non-local one. The largest LES domain is run for the full year of 2022, the two smaller ones only for April 2022. April 2022 in the Netherlands was characterized by a succession of cold high-pressure weather, synoptically driven weather, and fair weather conditions with shallow cumulus.[1]

All simulation domains are centered at the Cabauw meteorological mast, located at 51.971°N, 4.927°E. The LES domains use a horizontal resolution of 50 m. Vertically, a stretched grid is employed, which has a 25-m resolution at the surface and stretches to the model top at 3000 m.

The mesoscale simulation use a 2-km horizontal resolution, and the vertical resolution is 40 m near the surface and stretches to the top at 8000 m.

All simulations are performed as individual days, from midnight UTC to midnight UTC, with a spinup time of 6 h for the mesocale simulation and 1 h for the LES.

3.3 | Observation data

Observations of one-minute average wind speed during 2022 at the Cabauw meteorological mast (51.971°N, 4.927°E) were obtained via the Royal Netherlands Meteorological Institute (KNMI). At heights of 40, 80, 140, and 200 m, the tower has two booms oriented to approximately the north and west (±10° and ±250°, respectively). Each boom has a cup anemometer and wind vane to measure wind speed and wind direction. Depending on wind direction, therefore, the flow at the anemometers is disturbed by the tower. Figure 1 shows that there is a small difference in the wind increment distributions, spectra, and structure functions between the two booms. Correcting for the disturbance by the tower or filtering the data based on wind direction is not a straightforward procedure for one-minute data. Therefore, all analyses in this article will show data for both the anemometers, and differences between them will be regarded as observation uncertainty.

Missing values (their number ranging between 23 and 113, depending on height and boom) were linearly interpolated. The analyses focus mostly on the 80-m wind speed (36 missing values for the west boom, 49 for the north boom).

4 | RESULTS AND DISCUSSION

4.1 | Identifying key sensitivities in the simulated wind spectrum during April 2022

Previous studies with real-weather LES diagnose an underestimation of spectral energy in LES output at a period of several hours for wind (Schalkwijk *et al.*, 2015a) and solar irradiance (Stratum *et al.*, 2023). Given a typical advection speed of 10 m/s, these periods correspond to the meso-α scale (several hundreds of km). This suggests that adding these spatial scales in the modeling setup can improve the representation of these processes. To test this hypothesis, April 2022 was simulated in various model setups. All these setups consist of a 2-km horizontal resolution mesoscale simulation, with local- or non-local vertical diffusion, driving a 50 m horizontal resolution LES.

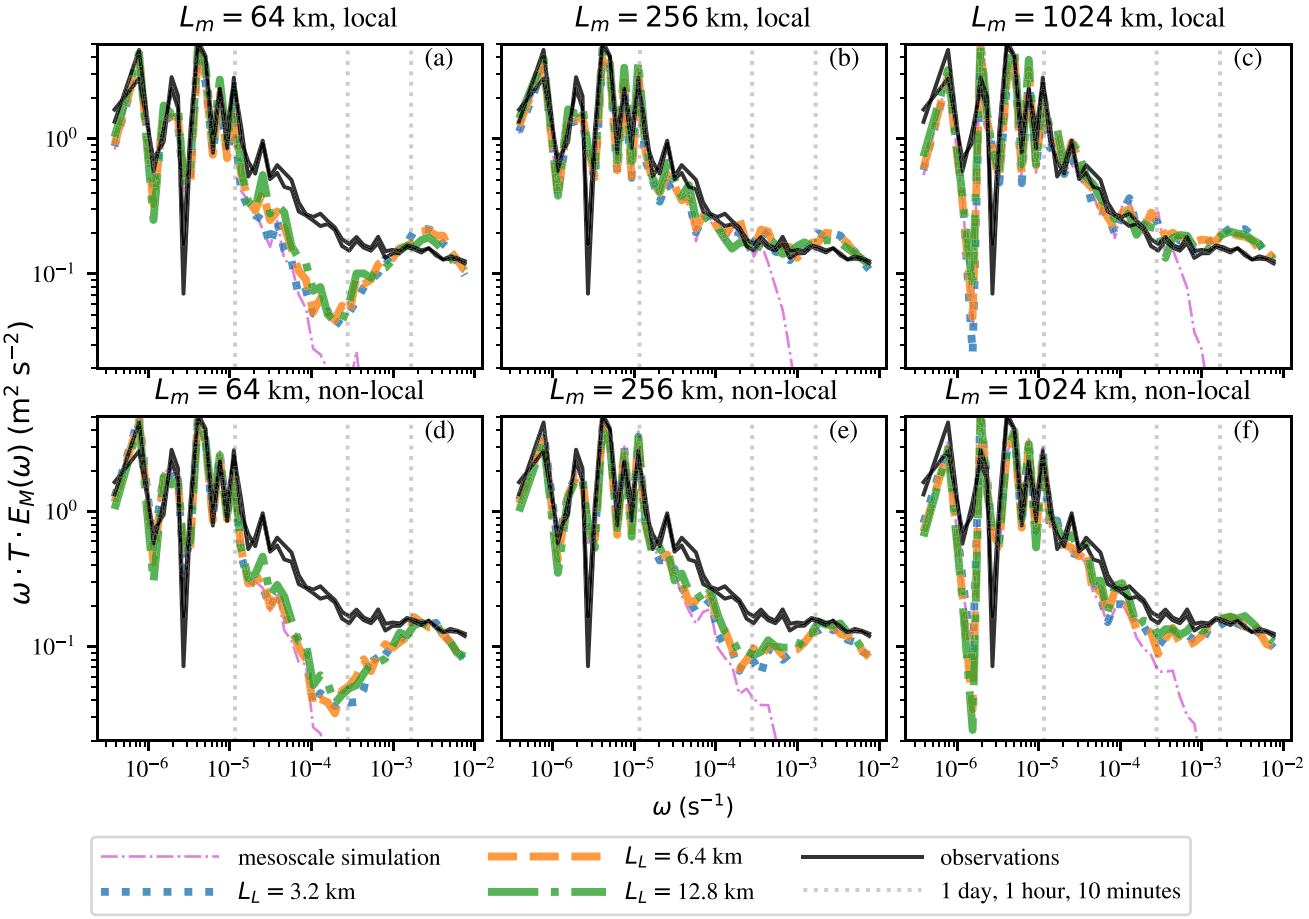

FIGURE 3 Spectra of the 80 m horizontal wind during April 2022 for different combinations mesoscale and LES domain sizes. The panels a-c (d-f) correspond to increasing domain size of the mesoscale simulation with a local (non-local) diffusion formulation, and the different lines in each panel correspond different LES domains nested in those mesoscale simulations. The spectrum of the mesoscale simulation itself is shown as a thin line, and the observations are identical in each panel.

To investigate the effect of domain size on the energy spectrum of the wind, the domain size of the mesoscale simulation (L_m) was varied between 64, 256, and 1024 km. Given the effective resolution of ERA5 of about 600 km (Bolgiani *et al.*, 2022), the smallest mesoscale simulation is therefore effectively driven by one ERA5 point, whereas the largest one is expected to capture heterogeneous boundary conditions from ERA5. The horizontal domain size of the LES (L_L) was varied between 3.2, 6.4, and 12.8 km.

Figure 3 shows the resulting energy spectra of the horizontal wind at 80-m height. Three time regimes can be identified, which reflect the simulation setup: the slowest regime (one month to one day, in the left plot) corresponds to the changing synoptic conditions, which are imposed by the ERA5 boundary conditions. All simulations show the same variance at these timescales. The second regime consists of timescales of approximately one day to 10 minutes. Given a typical advection speed of 10 m/s, this corresponds to spatial scales of several hundreds to several tens of kilometers, that is, scales that are comparable with or smaller than the effective resolution of ERA5. In this range, the simulated spectra respond strongly to the size of the mesoscale domain, but not to the size of the LES domain, confirming that the energy is produced by the mesoscale simulation. For both the local mesoscale diffusion scheme (top panels) and the non-local diffusion scheme (bottom panels), the simulations with the smallest mesoscale domain size show a clear energy minimum around a period of 1 h, similar to the spectra shown in Schalkwijk *et al.* (2015a) and Stratum *et al.* (2023). When moving to larger mesoscale domain sizes, this minimum gradually disappears and the spectrum is closer to the observed one. The spectrum also responds to the different formulations of vertical diffusion. In the local scheme, the simulations with L_m = 1024 km show a spectrum that has converged to the observations, whereas for the non-local scheme there is still a relatively small energy deficit around timescales of 1 h. This confirms the contrasting nature of these two diffusion schemes: the local scheme is less

diffusive and therefore permits more explicit convection, that is, more mesoscale variance, than the very diffusive non-local scheme.

In the final regime, at time scales below 10 minutes, the mesoscale simulations do not produce any variance (see the thin lines in Figure 3). Rather, the LES adds its turbulent fluctuations to the mesoscale inflow conditions. The magnitude of these fluctuations depends on the diffusion scheme of the mesoscale simulation. When driven by a mesoscale simulation with a local diffusion scheme (top panels), the energy is overestimated, whereas with a non-local diffusion scheme it represents the observations well. Among the different mesoscale and LES domains, there is little difference in energy at scales shorter than 10 min.

By simulating April 2022 in a large number of setups, we have now identified two main sensitivities in the energy spectrum of the wind in our coupled mesoscale–LES simulation setup: (1) the mesoscale domain size and (2) its formulation of vertical diffusion. Most importantly, Figure 3 shows that, by using a large enough mesoscale domain size, the observed wind spectrum across all timescales (synoptic to minutes) can be reproduced. It was also found that the size of the LES domain is less important in setting the mesoscale spectrum. Informed by these first results, the next section will study the sensitivities in the spectrum in more detail. Simulations of one year, with varying mesoscale domain size and mesoscale diffusion scheme but fixed LES domain size will be considered.

4.2 | Wind spectra and higher order wind statistics during the full year 2022

To substantiate the earlier findings and to extend the analyses to a wider range of weather conditions and seasons, we will now consider simulations of the full year of 2022, and add analyses of wind ramps and structure functions. Since the size of the mesoscale domain was identified as the most important factor in determining the spectrum, its domain size will again be varied between 64, 256, and 1024 km. Both local and non-local diffusion schemes will be used. The resolution of the mesoscale simulations is 2 km, and an LES of 256 horizontal grid points with a horizontal resolution of 50 m is used. This results in six full-year LES runs to be presented in this section.

Figure 4 shows the spectrum calculated based on the horizontal wind speed at 80-m height for the full year. Also, the spectra for day and night-time are shown separately in Figure 5. Considering the full-year spectra, the same qualitative picture emerges as for April 2022 (cf. Figure 3): an increased mesoscale domain size adds energy around timescales of 1 h. Furthermore, the local and non-local diffusion schemes respond differently to domain size: the

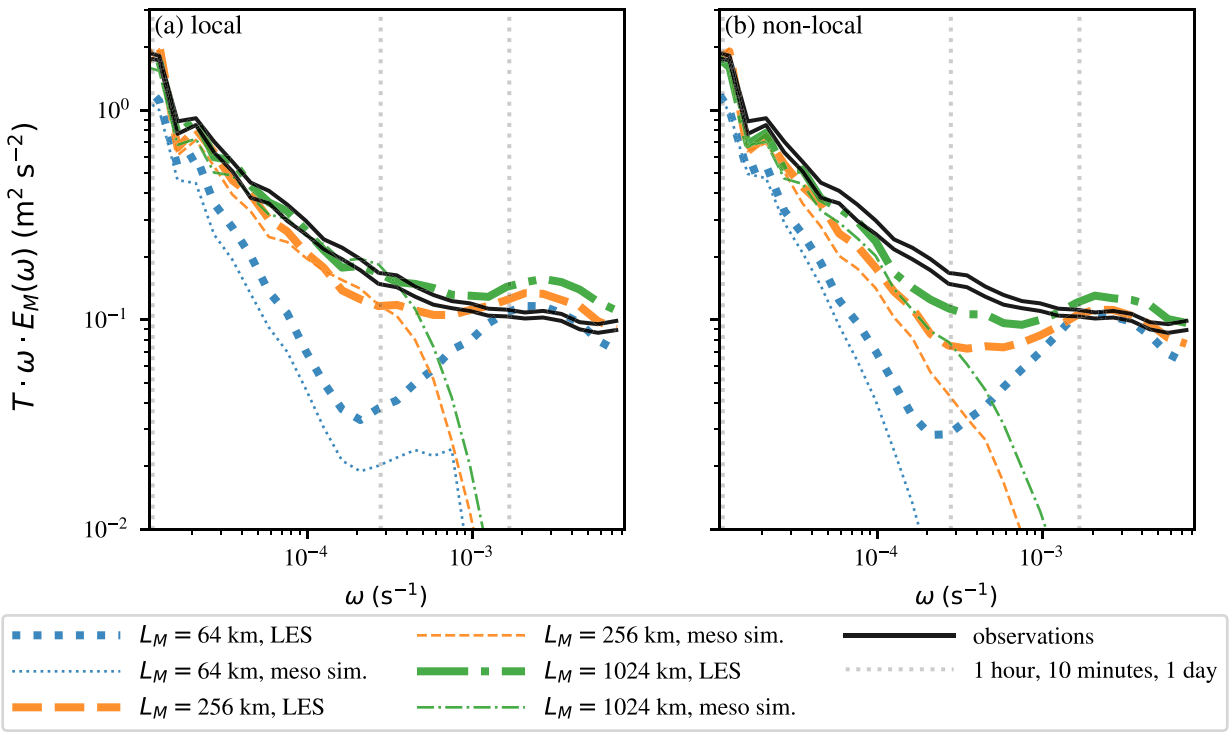

FIGURE 4 Spectra of the 80-m wind speed during 2022 for the different mesoscale domain sizes (indicated by different lines, thick lines for the LES, thin for the meosocale simulations), with (a) local diffusion and (b) non-local diffusion. The LES domain size is 12.8 km.

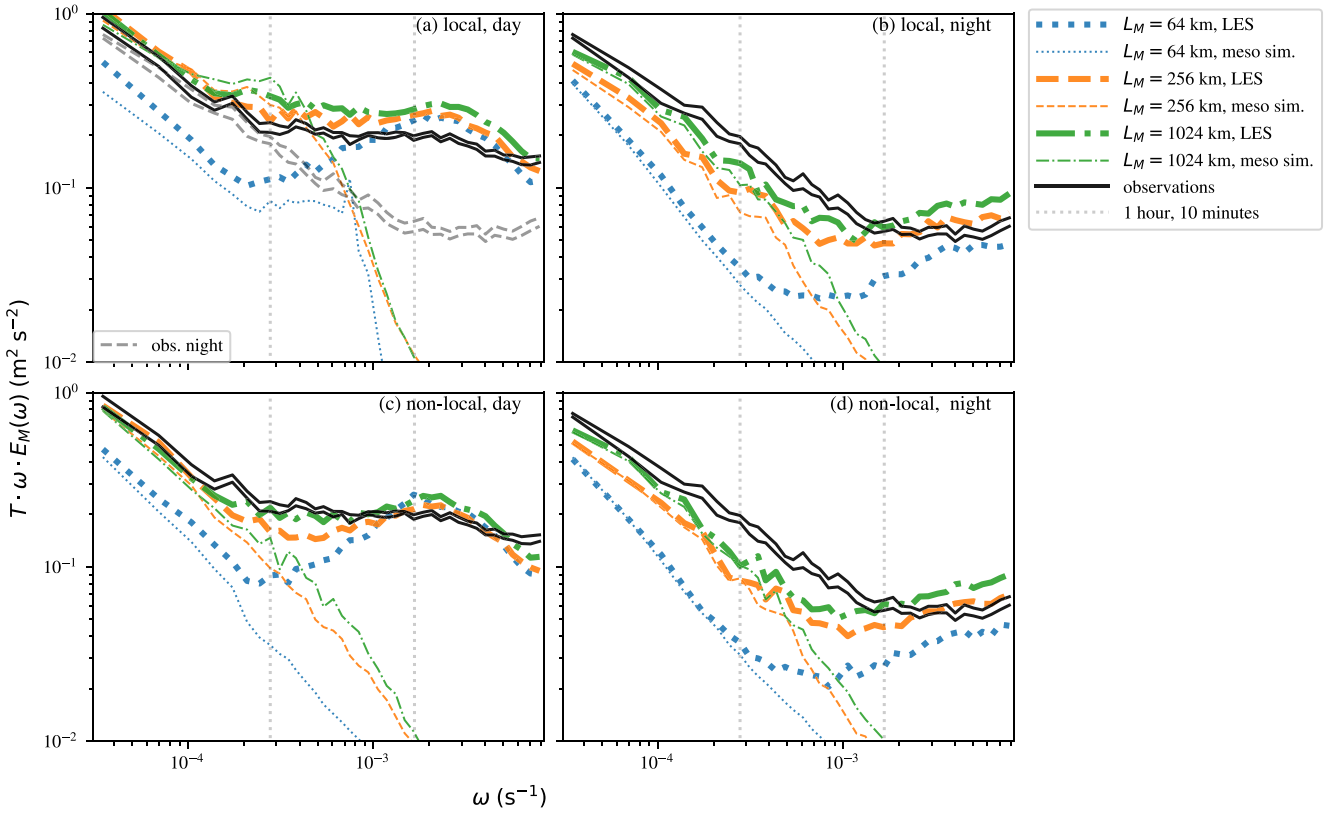

FIGURE 5 Spectra of the 80-m wind speed during 2022, averaged over daytime (0900–1700 UTC) and night-time (2100–0500 UTC). The different lines correspond to different mesoscale domain sizes, and both the LES spectra (domain size 12.8 km) and mesoscale spectra (thin lines) are shown. Panel (a) also shows the observed night-time spectrum, to indicate the day–night difference.

spectrum in the mesoscale converges to observations with a local diffusion scheme at $L_m = 1024$ km, but has not reached convergence with the non-local formulation. Furthermore, the LES shows too much variance below 10 minutes for the local diffusion scheme, but reproduces this part of the spectrum better when driven by a non-local diffusion mesoscale simulation. The variation of the spectra with height is not shown, but behaves qualitatively similarly to that presented in Larsén *et al.* (2016): at lower heights, the relative contribution of energy at scales shorter than roughly 10 min increases due to turbulence production by shear.

The separate day- and night-time spectra (Figure 5) are calculated as averaged spectra between 0900–1700 UTC and 2100–0500 UTC. Although this is arguably a crude way of filtering the data, because it neglects any seasonality in weather and day length, day and night already show marked differences. In the observations, the energy at scales shorter than approximately one hour is considerably higher during daytime than during night-time (see Figure 5a). This likely is the imprint of convective eddies in the boundary layer, which are a source of turbulence kinetic energy at these scales during the day. At night, contrastingly, the observed mesoscale spectrum is closer to $\omega^{-2/3}$ for a longer range of times, indicating that the turbulence cascade, rather than turbulence production, is the dominant mechanism. At scales below 10 minutes, the night-time spectra also depart from $\omega^{-2/3}$, possibly indicating the effect of turbulence production by shear. All LES runs capture this observed day–night contrast. Sub-one-minute resolved TKE profiles indicate similar qualitative behavior among the different simulations to that for the spectra (not shown). During daytime, the timescales around approximately one hour also show differences between the local and non-local mesoscale diffusion schemes. Namely, the simulations with the local scheme need smaller domain sizes to reproduce the observed spectrum. This again reflects the behavior of a local diffusion scheme: it (partially) resolves convective motions, whereas the non-local scheme is too diffusive to do this. It also highlights the two fundamentally different approaches to modeling in the gray zone of convection. As summarized by Honnert *et al.* (2020), such models either resemble a coarse LES, where turbulence is partially resolved, or a fine mesoscale model, where all turbulence should be handled by the

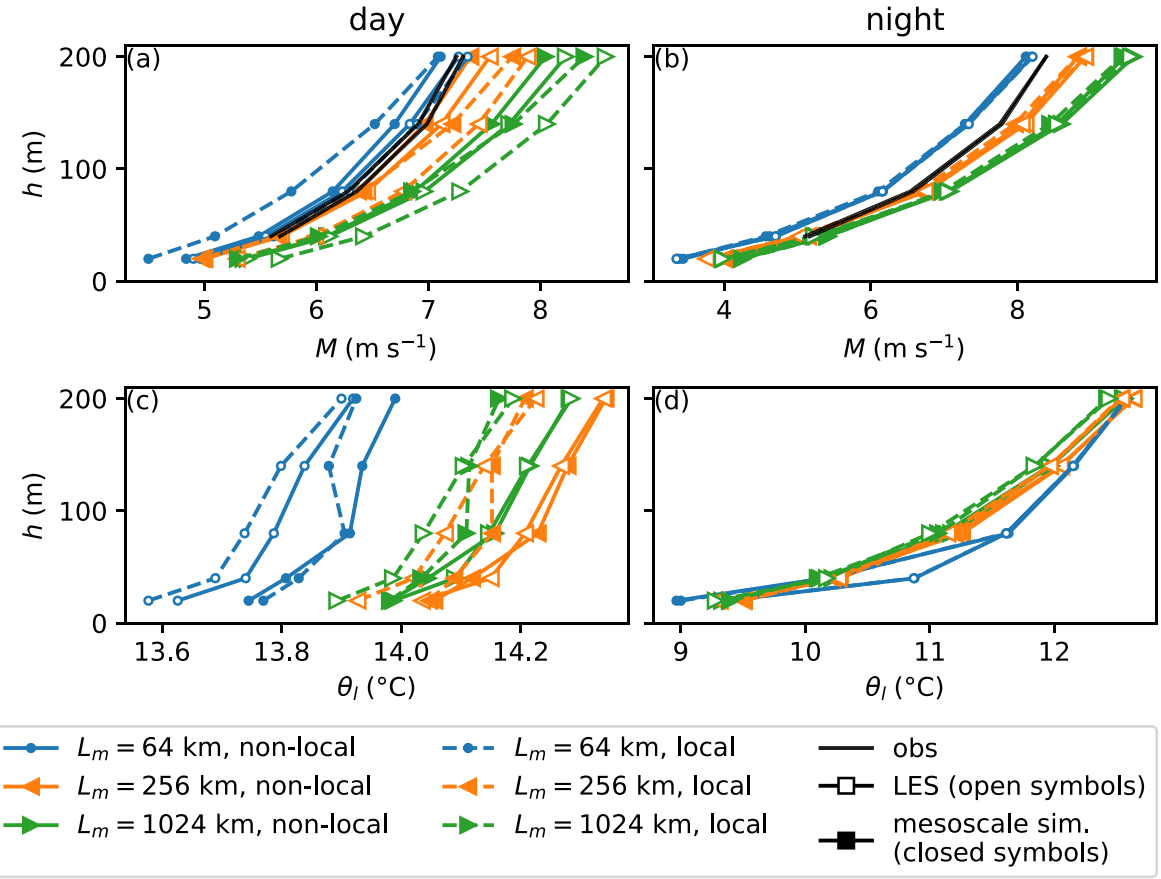

FIGURE 6 Observed and simulated mean profiles of wind speed during (a) day and (b) night for the mesoscale simulations (closed symbols), and the largest LES domain in each of those mesoscale simulations (open symbols). Non-local and local vertical diffusion is indicated by solid and dashed lines, respectively. Panels (c) and (d) show mean liquid potential temperature profiles for day and night, respectively. Day refers to 0900–1700 UTC and night to 2100–0500 UTC.

subgrid parametrizations. In simulations with grid spacing in the gray zone and an explicit treatment of convection, resolved variances become too strong and unrealistic (Zhou *et al.*, 2014) and are in general unreliable (Ching *et al.*, 2014). In the current study, similar behavior is observed in the mesoscale simulations with local diffusion: for the local scheme during daytime (Figure 5a), the variance around periods of about 1 h is overestimated in the largest mesoscale domain. The LES child could then introduce a "double counting" effect, because it adds its fluctuations to mesoscale structures that are already (partially) resolved.

At night, when there is less turbulence production (Figure 5b,c), the local and non-local schemes behave more similarly than during daytime. Whereas the small mesoscale domains result in an unrealistically deep spectral gap, the LES runs with the largest mesoscale domain reproduce the observed spectrum reasonably well. The LES variance below 10 min increases with increasing mesoscale domain size, and is slightly overestimated for the largest domain.

Most spectra show that, at scales below 10 min, the LES overestimates the variance, that is, becomes too turbulent. This overestimation increases with increasing size of the driving mesoscale domain. Also, it is most pronounced during daytime and when the LES is driven by the local mesoscale simulation. To elucidate the causes of the overestimation, it is useful to consider profiles of mean wind and potential temperature, because they are closely related to two important mechanisms of boundary-layer turbulence production, namely production by wind shear and convective instability. Figure 6 shows these profiles for the mesoscale simulations and the largest LES domain, for day and night separately. As expected, wind profiles are more sheared and temperature profiles more stable at night. In stably stratified flows (at night), the subgrid-scale model employed is expected to become inactive (Abkar & Moin, 2017). We expect that the night-time LES profiles observed in Figure 6 owe their substantial shear to this feature of the subgrid-scale model.

The wind profiles differ per domain size: for both day and night, wind speed is underestimated in the smallest

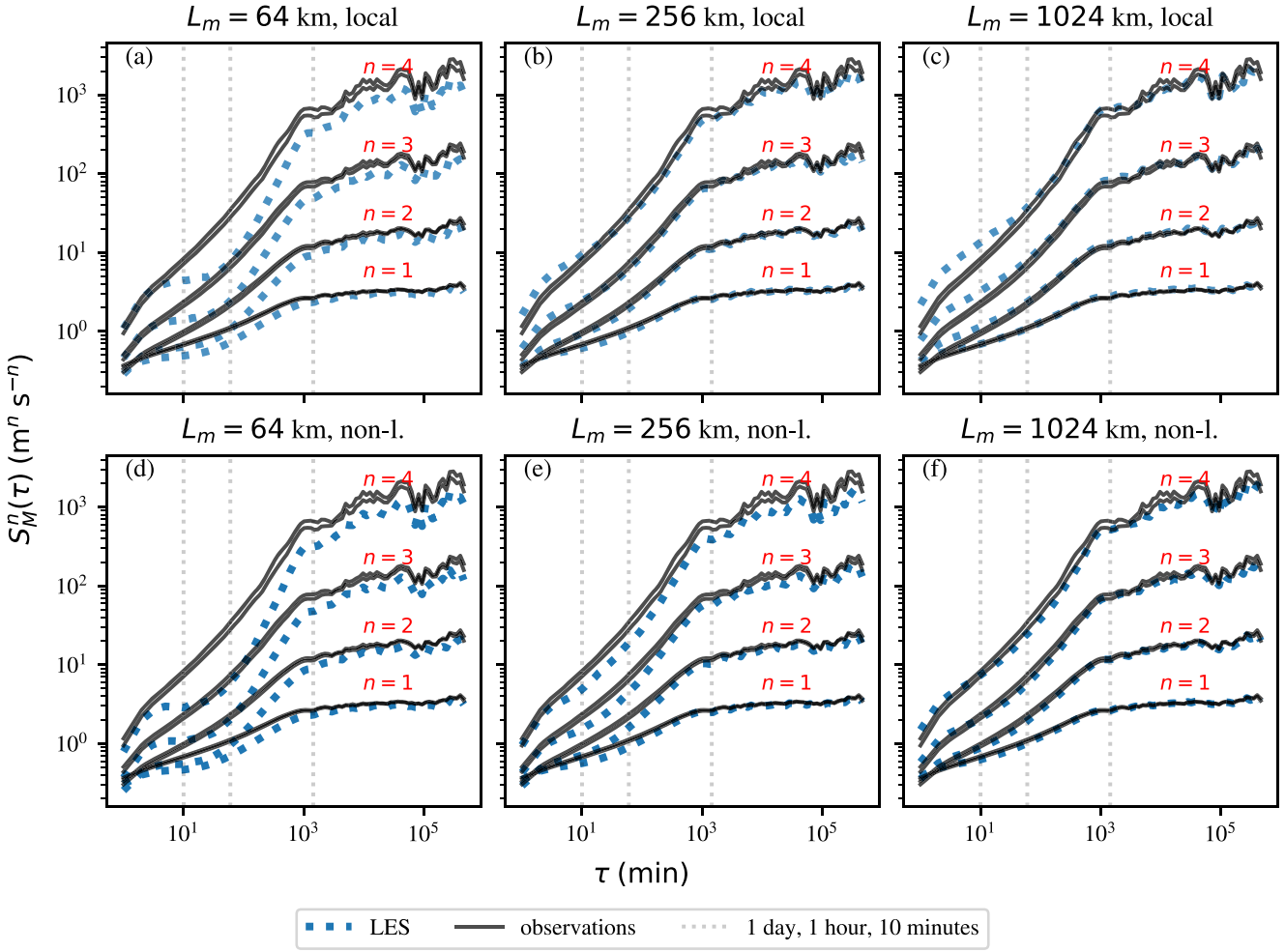

FIGURE 7 Structure functions for $n = 1, 2, 3, 4$ during 2022 as observed and simulated by the LES driven by the different mesoscale domains, with the (a–c) local and (d–f) non-local diffusion formulation.

mesoscale simulation and overestimated in the largest one. Also wind shear is stronger in the largest mesoscale simulations. The LES runs take their boundary conditions from these mesoscale simulations. With a higher mean wind and wind shear entering the LES domain, a larger production of turbulence can be expected in the LES. The temperature profiles differ relatively little between the domain sizes, but, during daytime, the simulations with a local scheme produce more unstable atmospheres. Therefore, the LES driven by these simulations receive a more unstable profile, which is conducive for more resolved turbulence.

These consideration provide a possible explanation for the observed overprediction of the sub-10-minute variance: because of stronger winds and more shear in the largest mesoscale simulations, the LES runs become prone to excessive turbulence production. Cause and effect, however, are not clearly separable: the positive wind bias can also be an effect of too rigorous turbulence (mixing air from aloft), instead of vice versa. Furthermore, because the simulations are a year long and therefore contain many different weather situations, it is difficult to find one clear mechanism that is responsible. For example, surface solar irradiance and surface energy fluxes are also expected to play a role.

The energy spectrum is related to the variance in the flow, but cannot give any information about the higher order moments. To quantify further the higher-order statistical agreement between observed and simulated wind, we now consider the structure functions, given by Equation (4), for n between 1 and 4 (Figure 7). All structure functions show an increasing value with lag time τ, which flattens above $\tau \approx 1000$ min. At high τ, the data become scarce, so the structure functions become noisy. Again, there is a large difference in the simulated structure functions. For $L_m = 64$ km in both the local and non-local schemes, a strong underestimation of all structure functions is found between several minutes and several hours, corresponding to the underestimation in the spectrum. This underestimation

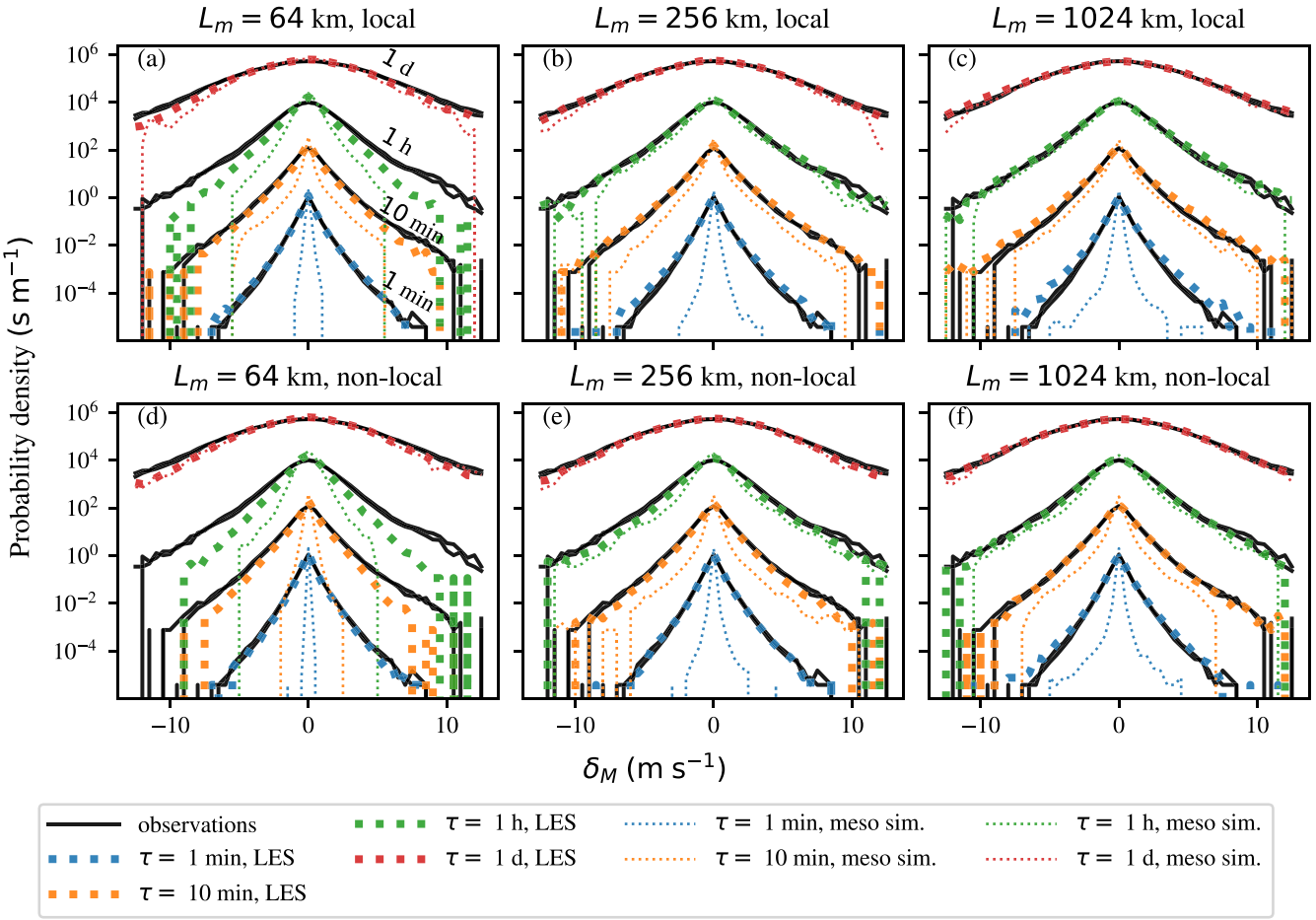

FIGURE 8 Probability distributions of wind increments at 80 m during 2022. Only data between −12.5 and 12.5 m/s are shown. The different panels show the results of both LES (thick dashed lines) driven by different mesoscale domain sizes and the mesoscale simulations themselves (thin dashed lines). Probability densities for lag times of 1 min, 10 min, 1 h, and 1 day are shown, and those for lag times above one minute are displaced successively by two decades for readability.

gradually decreases when moving to higher L_m. For LES runs driven by mesoscale simulations with the local diffusion scheme, the structure functions become overestimated at $L_m = 1024$ km. With the non-local scheme, they show good agreement with observations. This indicates that, apart from the variance, the higher-order moments also benefit from an increased mesoscale domain size.

These findings can be linked to a visual inspection of the distributions of wind increments (Equation 3). Figure 8 shows the wind increments distributions during 2022 for lag times of one minute, 10 minutes, one hour, and one day. The observed wind increments show their typical non-Gaussian distribution, which widens with increasing lag time. All simulations capture the general shapes of the distributions, but, depending on the lag time, there is a difference between the different mesoscale domain sizes and their diffusion schemes. Firstly, the distributions of the 1-min increments are captured well by most LES runs, also the ones with $L_m = 64$ km. This suggests that one-minute wind ramps are dominated by small-scale turbulent processes that can be captured in an LES without proper mesoscale inflow conditions. Only the LES driven by the largest mesoscale domain with the local diffusion scheme (Figure 8c) clearly overestimates the occurrence of one-minute wind ramps. This run also overestimates the variance and structure functions at short timescales (Figures 4 and 7).

To capture the distribution of the 10-minute and one-hour increments properly, larger mesoscale domain sizes are needed. Especially at a lag time of 1 h, the LES wind increments improve strongly with increasing mesoscale domain size. This is to be expected from the structure functions at $\tau = 1$ h (Figure 7), because they characterize the statistical moments of the wind-ramp distributions. It is furthermore interesting to note that the non-local mesoscale simulations alone (the thin dashed lines in Figure 8) do not capture these timescales fully. The turbulent fluctuations added by the LES are needed to reproduce the observed distributions.

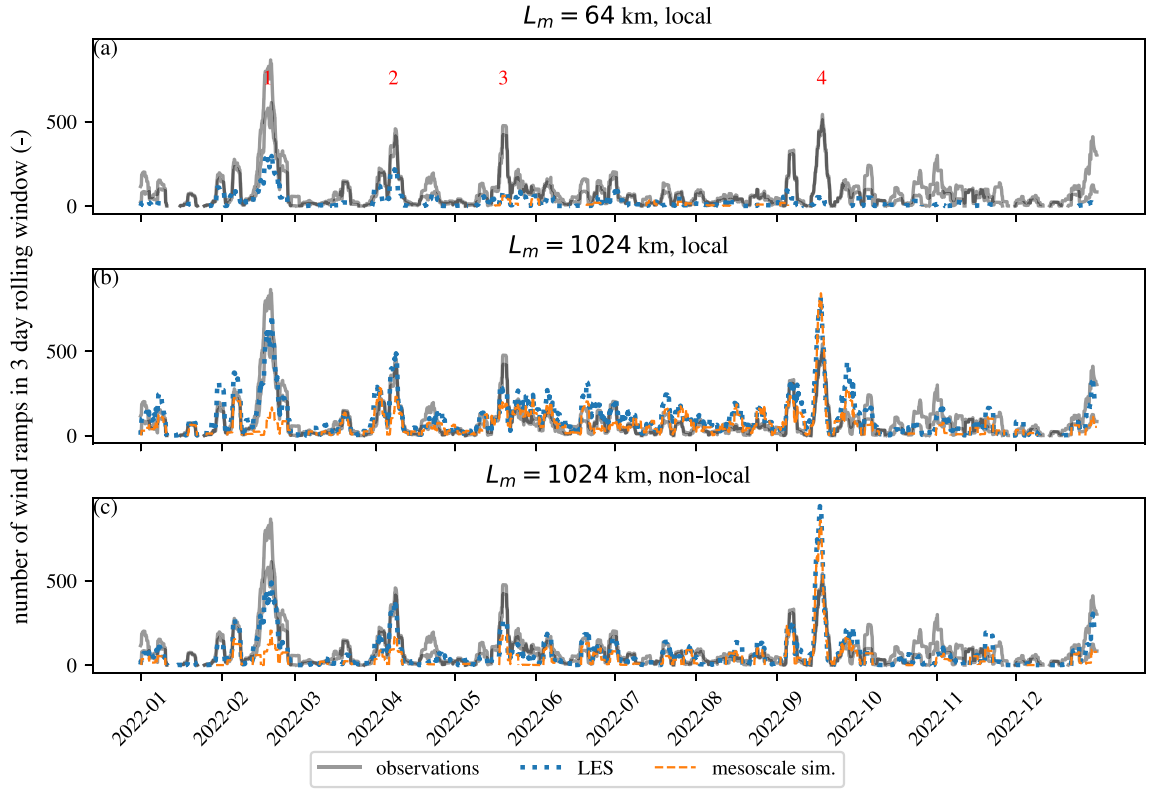

FIGURE 9 Time series of the number of 1-h wind ramps stronger than ±4 m/s in three-day rolling windows. Panel (a) shows $L_m = 64$ km with the local scheme (results for the non-local scheme are very similar and therefore not shown) and four periods of very high occurrence are labeled with numbers. Panels (b) and (c) show the same for $L_m = 1024$ km with the local and non-local schemes, respectively. All data are at 80-m height.

The wind increments have a similar interpretation to the spectra. Namely, the variability of the LES wind improves when the LES is driven by a large enough mesoscale simulation, which is in turn driven by large-scale weather data. In particular, the one-hour wind increments show increased realism. This is not surprising, because the variance added by the mesoscale simulation is centered around this period. The wind increment distributions confirm that this added variance is manifested correctly in the simulations, resulting in the characteristic long-tailed non-Gaussian shapes. Furthermore, they show that the extreme wind increments are the combined effect of mesoscale and turbulent fluctuations.

4.3 | Meteorological interpretation

All previous sections have given statistical validation of the wind as simulated by the LES runs and their parent mesoscale simulations. Because of transformation to the frequency domain (for spectral analysis) and temporal averaging (for the structure functions), information about specific meteorological events gets lost. In this section, therefore, we aim to explore the meaning of the previous findings in a phenomenological sense, rather than a statistical one. This will be done by considering extreme wind-ramp events that show improved representation with increasing mesoscale domain size.

To this end, Figure 9 shows time series of the total number of one-hour wind ramps stronger than ±4 m/s in rolling windows of 3 days throughout 2022, for observations and for the simulations with $L_m = 64$, 1024 km. This lag time, threshold, and averaging window were chosen to highlight the the differences between the mesoscale simulation and LES, and between the local and non-local schemes.

The curves in Figure 9 can be interpreted as wind-ramp occurrence densities. The previous (statistical) analyses have shown that the simulations capture the wind-ramp probability densities to varying degrees; Figure 9 is meant to show how the timing (or correlation) is captured. In general, the simulations capture the timing of periods of high wind ramp density fairly well. Most observed peaks, which represent clustered wind ramps, are also present in the simulations. The magnitude of the peaks, however, differs per simulation type. The LES driven by the mesoscale simulation with $L_m = 64$ km (top panel) underestimates the wind-ramp occurrence, whereas by adding a large

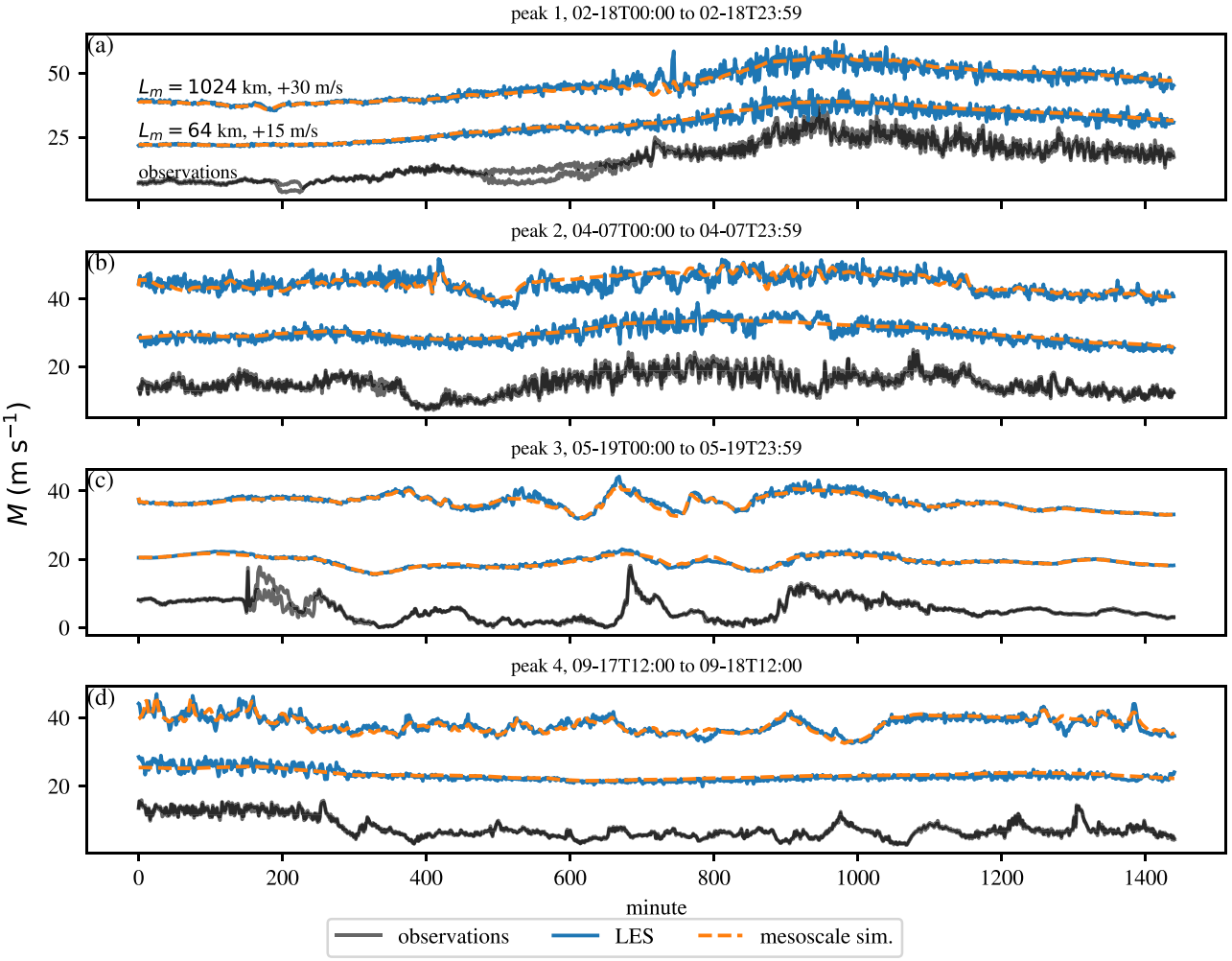

FIGURE 10 Time series of the 80-m wind speed during 24 hours surrounding the four periods labeled in Figure 9. Only data for the non-local scheme are shown, and the simulated time series are displaced by 15 m/s (for the small mesoscale domain) and 30 m/s (for the large mesoscale domain) for readability (as indicated in panel [a]).

mesoscale simulation (middle and bottom panels) the peaks are reproduced more realistically. The simulations where the LES is driven by a mesoscale simulation with the local scheme seem to overestimate wind-ramp occurrence in the summer months, whereas with the non-local scheme these periods are captured accurately. This could be a manifestation of excessive convection in the local simulation, especially prevalent during summer months with low mean wind speeds and strong surface heating.

Four periods of very high wind-ramp occurrence are highlighted in Figure 9 with numbers, for further interpretation, and Figure 10 shows the wind time series during those periods. Only data for the non-local scheme with $L_m = 64,\ 1024$ km are shown. The following interpretations have been made using weather maps from KNMI,[2], KNMI monthly weather overviews,[3], and NASA Worldview,[4] all last accessed on October 16, 2025.

Peak 1 (February 18) corresponds to the extratropical storm *Eunice*, which brought very strong surface winds (Volonté *et al.*, 2024). It is striking to see that, for both the local and non-local schemes, the mesoscale simulation alone does not capture the wind extremes. When the LES is added, however, the pattern and magnitude of the observed wind are captured reasonably well. This suggests that storm situations like this can be described as a slow-varying synoptic component with turbulent fluctuations, that is, a weak mesoscale component. Interestingly, an early point of criticism on the existence of a spectral gap, as hypothesized by Van der Hoven (1957), was that the underlying wind data would have been measured in very strong wind (hurricane) conditions (Lovejoy & Schertzer, 2013; Vinnichenko, 1970).

Peak 2 (April 7) also occurred during strong synoptic forcing, with the passage of a low-pressure system north of the Netherlands and a complex frontal situation. Here, we see that the mesoscale simulation and the LES are roughly equally important in representing the wind ramps well.

The magnitude of peak 3 (May 19) is not captured completely by any of the simulations. It occurred during low mean wind conditions, under the influence of a high-pressure system and the presence of convective storms. The characteristic peaks in wind speed (e.g. around minute 700 in Figure 10) are not clearly present in the simulations.

Finally, peak 4 (September 17) seems to be dominated by mesoscale effects: there is a large difference between the simulations with $L_m = 64$ km and $L_m = 1024$ km. The simulation with $L_m = 1024$ km shows a similar pattern of peaks in wind speed to the observations, although the timing is wrong.

A complete meteorological analysis of the simulated wind time series is outside the scope for this study. However, the four situations described above illustrate that clustered wind ramps occur under a range of different weather conditions, in which the relative importance of mesoscale and local turbulence varies depending on the large-scale synoptic conditions.

5 | CONCLUSION

In their study of a year-long periodic LES, Schalkwijk *et al.* (2015a) concluded that, to resolve the missing mesoscale processes in their simulation, LES domains of about 200 km are needed. Such large domains are computationally expensive for year-long LES runs, especially in an operational setting, where simulations must be completed faster than real time. The current study therefore explored Schalkwijk's hypothesis by using mesoscale-type simulations as parent to a much smaller open boundary condition LES. The main finding is that the missing mesoscales can indeed be introduced in the LES by using a large enough mesoscale simulation to drive it. As shown by the wind spectrum, increasing the size of the mesoscale domain increasingly adds variance around scales of one hour. For mesoscale domains of 1024 km by 1024 km, the LES spectrum can reproduce the observed spectrum satisfactorily across all scales. This is in line with (Bolgiani *et al.*, 2022), who find that the effective resolution of ERA5 is around 600 km in the midlatitudes, and that ERA5 does not capture the transition of the synoptic spectrum ($\propto k^{-3}$) to the mesoscale spectrum ($\propto k^{-5/3}$). By adding a mesoscale simulation that does capture scales below 600 km, and therefore the mesoscale $\propto k^{-5/3}$ regime, the LES can introduce its fluctuations on sub-10-minute turbulence scales, and then all atmospheric scales are represented.

The LES wind spectrum is furthermore sensitive to the formulation of vertical diffusion in the parent mesoscale simulation. When using a local vertical diffusion scheme, convection in the mesoscale simulation is partially resolved and is known to become too energetic and unreliable (Ching *et al.*, 2014; Zhou *et al.*, 2014). In these simulations, the LES child also becomes overly turbulent below timescales of 10 minutes, possibly due to double counting of the turbulence. Peña and Mirocha (2024) also find increased variance in their year-long LES run (albeit between 1 hour and 20 minutes) and attribute it to similar causes. Furthermore, in the simulations presented here, the mean wind speed and wind shear increase with mesoscale domain size. This is an undesirable effect, which also influences turbulence levels in the LES, because of increased turbulence production by shear.

The difference between the local and non-local schemes is, in effect, a manifestation of the gray-zone problem: should turbulence in mesoscale models be resolved or not? Whereas, classically, the "double counting" issue refers to representing the same turbulence scales resolved both on the grid and in the parameterizations, in this study it refers to turbulent scales being resolved by both the mesoscale simulation and the LES.

Apart from the spectrum, the structure functions and distributions of wind increments were analyzed, which provides information the spectrum cannot give. Also, here, it was found that the LES wind statistics improve when adding a large enough mesoscale simulation as parent. As expected, the timescales around one hour improve especially. In line with the results from the spectrum, the LES overestimates the higher order structure functions when driven by a mesoscale simulation with local diffusion.

Finally, several meteorological events that feature strong mesoscale wind ramps were analyzed. These show that the temporal representation of the wind ramps agrees qualitatively with observations.

The methods of analysis in this study are mostly statistical and rely on long time series of $\mathcal{O}(10^5)$ data points that span all seasons. This fits with our approach of employing LES as a "real-weather" model, in which the primary goal is a sane simulation of all possible weather conditions with one single simulation setup. This approach necessarily comes at the expense of the representation, and understanding, of individual days or specific flow regimes. Studying the role of mesoscale processes in more specific cases, to complement our statistical approach, might therefore be an interesting route for further research. Furthermore, variables other than wind time series have not been considered in this study. Extending it to other variables, most notably clouds and radiation, is a relevant topic for further research too.

ACKNOWLEDGMENTS

The authors thank Mariska Koning from the Royal Netherlands Meteorological Institute for her advice and for providing the observation data.

CONFLICT OF INTEREST STATEMENT

The authors declare no conflicts of interest.

DISCLOSURE

The authors have nothing to report.

DATA AVAILABILITY STATEMENT

The LES data and code to reproduce the figures are available through Zenodo (Postema, 2025: DOI https://doi.org/10.5281/zenodo.16084592). The observation data are available upon request from the Royal Netherlands Meteorological Institute via cabauw.insitu@knmi.nl.

The data that support the findings of this study are openly available in Representing the Mesoscale Wind Spectrum in Real-Weather LES at https://zenodo.org/records/16084592.

ENDNOTES

[1]https://www.knmi.nl/nederland-nu/klimatologie/maand-en-seizoensoverzichten/2022/april, last accessed October 3, 2025.
[2]https://www.knmi.nl/nederland-nu/klimatologie/daggegevens/weerkaarten.
[3]https://www.knmi.nl/nederland-nu/klimatologie/maand-en-seizoensoverzichten.
[4]https://worldview.earthdata.nasa.gov.

ORCID

Bernard Postema https://orcid.org/0009-0007-8498-5490

REFERENCES

Abkar, M., Bae, H.J. & Moin, P. (2016) Minimum-dissipation scalar transport model for large-eddy simulation of turbulent flows. *Physical Review Fluids*, 1(4), 041701. Available from: https://doi.org/10.1103/PhysRevFluids.1.041701

Abkar, M. & Moin, P. (2017) Large-eddy simulation of thermally stratified atmospheric boundary-layer flow using a minimum dissipation model. *Boundary-Layer Meteorology*, 165(3), 405–419. Available from: https://doi.org/10.1007/s10546-017-0288-4

Alonzo, B., Cassas, M., Raynaud, L., Verzijlbergh, R., Houf, D., Baas, P. et al. (2022) *Smart4res: report on improved NWP with higher spatial and temporal resolution*. https://www.smart4res.eu/wp-content/uploads/2023/01/Smart4RES_Deliverable_D2.2.pdf

Arakawa, A. & Lamb, V.R. (1977) *Computational Design of the Basic Dynamical Processes of the UCLA General Circulation Model*, Vol. 17, pp. 173–265. New York: Academic Press.

Arthur, R.S., Mirocha, J.D., Marjanovic, N., Hirth, B.D., Schroeder, J.L., Wharton, S. et al. (2020) Multi-scale simulation of wind farm performance during a frontal passage. *Atmosphere*, 11, 245. Available from: https://doi.org/10.3390/atmos11030245

Baas, P., Verzijlbergh, R., Dorp, P.V. & Jonker, H.J.J. (2023) Investigating energy production and wake losses of multi-gigawatt offshore wind farms with atmospheric large-eddy simulation. *Wind Energy Science*, 8, 787–805. Available from: https://doi.org/10.5194/wes-8-787-2023

Bauer, P., Thorpe, A. & Brunet, G. (2015) The quiet revolution of numerical weather prediction.

Bieringer, P.E., Piña, A.J., Lorenzetti, D.M., Jonker, H.J., Sohn, M.D., Annunzio, A.J. et al. (2021) A graphics processing unit (GPU) approach to large eddy simulation (LES) for transport and contaminant dispersion. *Atmosphere*, 12, 890. Available from: https://doi.org/10.3390/atmos12070890

Bolgiani, P., Calvo-Sancho, C., Díaz-Fernández, J., Quitián-Hernández, L., Sastre, M., Santos-Muñoz, D. et al. (2022) Wind kinetic energy climatology and effective resolution for the era5 reanalysis. *Climate Dynamics*, 59, 737–752. Available from: https://doi.org/10.1007/s00382-022-06154-y

Callies, J., Ferrari, R. & Bühler, O. (2014) Transition from geostrophic turbulence to inertia-gravity waves in the atmospheric energy spectrum. *Proceedings of the National Academy of Sciences of the United States of America*, 111, 17033–17038. Available from: https://doi.org/10.1073/pnas.1410772111

Charnock, H. (1955) Wind stress on water: an hypothesis wind stress on a water surface. *Quarterly Journal of the Royal Meteorological Society*, 81, 639–640.

Cheneka, B.R., Watson, S.J. & Basu, S. (2020) A simple methodology to detect and quantify wind power ramps. *Wind Energy Science*, 5, 1731–1741. Available from: https://doi.org/10.5194/wes-5-1731-2020

Ching, J., Rotunno, R., Lemone, M., Martilli, A., Kosovic, B., Jimenez, P.A. et al. (2014) Convectively induced secondary circulations in fine-grid mesoscale numerical weather prediction models. *Monthly Weather Review*, 142, 3284–3302. Available from: https://doi.org/10.1175/MWR-D-13-00318.1

De Roode, S.R., Duynkerke, P.G. & Jonker, H.J.J. (2004) Large-eddy simulation: how large is large enough? *Journal of the Atmospheric Sciences*, 61, 403–421.

DeMarco, A. & Basu, S. (2018) On the tails of the wind ramp distributions. *Wind Energy*, 21, 892–905. Available from: https://doi.org/10.1002/we.2202

der Van Hoven, I. (1957) Power spectrum of horizontal wind speed in the frequency range from .0007 to 900 cycles per hour. *Journal of Meteorology*, 14, 160–164.

ECMWF. (2017) *Ifs manual part iv: Physical processes. ifs documentation cy43r3. technical report*. https://www.ecmwf.int/en/elibrary/80320-ifs-documentation-cy43r3-part-iv-physical-processes

Frisch, U. (1995) *Turbulence*. Cambridge: Cambridge University Press.

Gilbert, C., Messner, J.W., Pinson, P., Trombe, P.J., Verzijlbergh, R., van Dorp, P. et al. (2020) Statistical post-processing of turbulence-resolving weather forecasts for offshore wind power forecasting. *Wind Energy*, 23, 884–897. Available from: https://doi.org/10.1002/we.2456

Grabowski, W.W. (1998) Toward cloud resolving modeling of large-scale tropical circulations: a simple cloud microphysics parameterization. *Journal of the Atmospheric Sciences*, 55(21), 3283–3298. Available from: https://doi.org/10.1175/1520-0469(1998)055<3283:TCRMOL>2.0.CO;2

Haupt, S.E., Kosovic, B., Shaw, W., Berg, L.K., Churchfield, M., Cline, J. et al. (2019) On bridging a modeling scale gap: mesoscale

to microscale coupling for wind energy. *Bulletin of the American Meteorological Society*, 100, 2533–2549. Available from: https://doi.org/10.1175/BAMS-D-18-0033.1

Heerwaarden, C.C.V., Stratum, B.J.V., Heus, T., Gibbs, J.A., Fedorovich, E. & Mellado, J.P. (2017) Microhh 1.0: a computational fluid dynamics code for direct numerical simulation and large-eddy simulation of atmospheric boundary layer flows. *Geoscientific Model Development*, 10, 3145–3165. Available from: https://doi.org/10.5194/gmd-10-3145-2017

Heinze, R., Dipankar, A., Henken, C.C., Moseley, C., Sourdeval, O., Trömel, S. et al. (2017) Large-eddy simulations over Germany using icon: a comprehensive evaluation. *Quarterly Journal of the Royal Meteorological Society*, 143, 69–100. Available from: https://doi.org/10.1002/qj.2947

Hersbach, H., Bell, B., Berrisford, P., Hirahara, S., Horányi, A., Muñoz-Sabater, J. et al. (2020) The era5 global reanalysis. *Quarterly Journal of the Royal Meteorological Society*, 146, 1999–2049. Available from: https://doi.org/10.1002/qj.3803

Heus, T., Van Heerwaarden, C.C., Jonker, H.J., Siebesma, A.P., Axelsen, S., Van Den Dries, K. et al. (2010) Formulation of the Dutch atmospheric large-eddy simulation (dales) and overview of its applications. *Geoscientific Model Development*, 3, 415–444. Available from: https://doi.org/10.5194/gmd-3-415-2010

Ho, Y.F., Hengl, T. & Parente, L. (2023) Ensemble digital terrain model (EDTM) of the world. Available from: https://doi.org/10.5281/zenodo.7676373

Hogan, R.J. & Bozzo, A. (2018) A flexible and efficient radiation scheme for the ECMWF model. *Journal of Advances in Modeling Earth Systems*, 10(8), 1990–2008. Available from: https://doi.org/10.1029/2018MS001364

Holtslag, A. & Boville, B. (1993) Local versus nonlocal boundary-layer diffusion in a global climate model. *Journal of Climate*, 6, 1825–1845.

Honnert, R., Efstathiou, G.A., Beare, R.J., Ito, J., Lock, A., Neggers, R. et al. (2020) The atmospheric boundary layer and the gray zone of turbulence: a critical review. *Journal of Geophysical Research: Atmospheres*, 125, e2019JD030317. Available from: https://doi.org/10.1029/2019JD030317

Kantharaju, J., Storey, R., Julian, A., Delaunay, F. & Michaud, D. (2023) Wind resource modelling of entire sites using large eddy simulation. *Journal of Physics: Conference Series*, 2507, 012015.

Khairoutdinov, M.F. & Randall, D.A. (2003) Cloud resolving modeling of the arm summer 1997 IOP: model formulation, results, uncertainties, and sensitivities. *Journal of the Atmospheric Sciences*, 60(4), 607–625.

Kolmogorov, A. (1941) Local structure of turbulence in an incompressible viscous fluid at very large Reynolds numbers. *Doklady Akademii Nauk SSSR*, 30, 299–301.

Larsén, X.G., Larsen, S.E. & Petersen, E.L. (2016) Full-scale spectrum of boundary-layer winds. *Boundary-Layer Meteorology*, 159, 349–371. Available from: https://doi.org/10.1007/s10546-016-0129-x

Lean, H.W., Theeuwes, N.E., Baldauf, M., Barkmeijer, J., Bessardon, G. & Blunn, L. (2024) The hectometric modelling challenge: gaps in the current state of the art and ways forward towards the implementation of 100-m scale weather and climate models.

Lilley, M., Lovejoy, S., Strawbridge, K.B., Schertzer, D. & Radkevich, A. (2008) Scaling turbulent atmospheric stratification. II: spatial stratification and intermittency from Lidar data. *Quarterly Journal of the Royal Meteorological Society*, 134, 301–315. Available from: https://doi.org/10.1002/qj.202

Lindborg, E. (1999) Can the atmospheric kinetic energy spectrum be explained by two-dimensional turbulence? *Journal of Fluid Mechanics*, 388, 259–288. Available from: https://doi.org/10.1017/S0022112099004851

Lorenz, E.N. (1969) The predictability of a flow which possesses many scales of motion. *Tellus*, 21, 289–307. Available from: https://doi.org/10.1111/j.2153-3490.1969.tb00444.x

Lovejoy, S. & Schertzer, D. (2013) *The weather and climate: emergent laws and multifractal cascades*. Cambridge: Cambridge University Press.

Maronga, B., Banzhaf, S., Burmeister, C., Esch, T., Forkel, R., Fröhlich, D. et al. (2020) Overview of the palm model system 6.0. *Geoscientific Model Development*, 13, 1335–1372. Available from: https://doi.org/10.5194/gmd-13-1335-2020

Nastrom, G.D. & Gage, K.S. (1983) A first look at wavenumber spectra from gasp data. *Tellus. Series A, Dynamic Meteorology and Oceanography*, 35 A, 383–388. Available from: https://doi.org/10.1111/j.1600-0870.1983.tb00213.x

Nastrom, G.D. & Gage, K.S. (1985) A climatology of atmospheric wavenumber spectra of wind and temperature observed by commercial aircraft. *Journal of the Atmospheric Sciences*, 42, 950–960.

Nastrom, G.D., Gage, K.S. & Jasperson, W.H. (1984) Kinetic energy spectrum of large- and mesoscale atmospheric processes. *Nature*, 310, 36–38.

Oldbaum. (2019) *Wind resource assessment hollandse kust (noord) wind farm zone*. https://offshorewind.rvo.nl/files/view/9717fb65-79ab-4966-92e2-a73c856c18c9/hkn_20191022_oldbaum_wra-oct19-f.pdf Accessed 2nd October 2010.

Optis, M., Monahan, A. & Bosveld, F.C. (2016) Limitations and breakdown of Monin–Obukhov similarity theory for wind profile extrapolation under stable stratification. *Wind Energy*, 19(6), 1053–1072. Available from: https://doi.org/10.1002/we.1883

Panofsky, H.A. & van der Hoven, I. (1955) Spectra and cross-spectra of velocity components in the mesometeorological range. *Quarterly Journal of the Royal Meteorological Society*, 81, 603–606. Available from: https://doi.org/10.1002/qj.49708135010

Peña, A. & Mirocha, J.D. (2024) One-year-long turbulence measurements and modeling using large-eddy simulation domains in the weather research and forecasting model. *Applied Energy*, 363, 123069. Available from: https://doi.org/10.1016/j.apenergy.2024.123069

Postema, B. (2025) Data and code for representing the mesoscale wind spectrum in real-weather large-eddy simulation. https://doi.org/10.5281/zenodo.16084592

Postema, B., Verzijlbergh, R.A., van Dorp, P., Baas, P. & Jonker, H.J.J. (2025) Estimating long-term annual energy production from shorter-time-series data: methods and verification with a 10-year large-eddy simulation of a large offshore wind farm. *Wind Energy Science*, 10, 1471–1484. Available from: https://doi.org/10.5194/wes-10-1471-2025

Rai, R.K., Berg, L.K., Kosović, B., Haupt, S.E., Mirocha, J.D., Ennis, B.L. et al. (2019) Evaluation of the impact of horizontal grid spacing in terra incognita on coupled mesoscale-microscale simulations using the wrf framework. *Monthly Weather Review*, 147, 1007–1027. Available from: https://doi.org/10.1175/MWR-D-18-0282.1

Rozema, W., Bae, H.J., Moin, P. & Verstappen, R. (2015) Minimum-dissipation models for large-eddy simulation. *Physics of Fluids*, 27. Available from: https://doi.org/10.1063/1.4928700

Sauer, J.A. & Muñoz-Esparza, D. (2020) The fasteddy®; resident-gpu accelerated large-eddy simulation framework: model formulation, dynamical-core validation and performance benchmarks. *Journal of Advances in Modeling Earth Systems*, 12, e2020MS002100. Available from: https://doi.org/10.1029/2020MS002100

Schalkwijk, J., Griffith, E.J., Post, F.H. & Jonker, H.J. (2012) High-performance simulations of turbulent clouds on a desktop pc. *Bulletin of the American Meteorological Society*, 93, 307–314. Available from: https://doi.org/10.1175/BAMS-D-11-00059.1

Schalkwijk, J., Jonker, H.J., Siebesma, A.P. & Bosveld, F.C. (2015a) A year-long large-eddy simulation of the weather over CABAUW: an overview. *Monthly Weather Review*, 143, 828–844. Available from: https://doi.org/10.1175/MWR-D-14-00293.1

Schalkwijk, J., Jonker, H.J., Siebesma, A.P. & Meijgaard, E.V. (2015b) Weather forecasting using GPU-based large-eddy simulations. *Bulletin of the American Meteorological Society*, 96, 715–723. Available from: https://doi.org/10.1175/BAMS-D-14-00114.1

Schemann, V., Ebell, K., Pospichal, B., Neggers, R., Moseley, C. & Stevens, B. (2020) Linking large-eddy simulations to local cloud observations. *Journal of Advances in Modeling Earth Systems*, 12, e2020MS002209. Available from: https://doi.org/10.1029/2020MS002209

Schepers, G., Dorp, P.V., Verzijlbergh, R., Baas, P. & Jonker, H. (2021) Aeroelastic loads on a 10 mw turbine exposed to extreme events selected from a year-long large-eddy simulation over the north sea. *Wind Energy Science*, 6, 983–996. Available from: https://doi.org/10.5194/wes-6-983-2021

Schertzer, D. & Lovejoy, S. (2004) Uncertainty and predictability in geophysics: Chaos and multifractal insights. *State of the Planet, Frontiers and Challenges in Geophysics*, 150, 317–334.

Sim, S.K., Maass, P. & Roman, H.E. (2024) Distributions and correlation properties of offshore wind speeds and wind speed increments. *Boundary-Layer Meteorology*, 190, 48. Available from: https://doi.org/10.1007/s10546-024-00889-3

Stevens, R.J., Graham, J. & Meneveau, C. (2014) A concurrent precursor inflow method for large eddy simulations and applications to finite length wind farms. *Renewable Energy*, 68, 46–50. Available from: https://doi.org/10.1016/j.renene.2014.01.024

Storey, R. & Rauffus, R. (2024) Mesoscale-coupled large eddy simulation for wind resource assessment. *Journal of Physics: Conference Series*, 2767(5), 052040.

Stratum, B.J.V., Heerwaarden, C.C.V. & de Arellano, J.V.G. (2023) The benefits and challenges of downscaling a global reanalysis with doubly-periodic large-eddy simulations. *Journal of Advances in Modeling Earth Systems*, 15, e2023MS003750. Available from: https://doi.org/10.1029/2023MS003750

Suter, I., Grylls, T., Sützl, B.S., Owens, S.O., Wilson, C.E. & Reeuwijk, M.V. (2022) Udales 1.0: a large-eddy simulation model for urban environments. *Geoscientific Model Development*, 15, 5309–5335. Available from: https://doi.org/10.5194/gmd-15-5309-2022

Talbot, C., Bou-Zeid, E. & Smith, J. (2012) Nested mesoscale large-eddy simulations with WRF: performance in real test cases. *Journal of Hydrometeorology*, 13, 1421–1441. Available from: https://doi.org/10.1175/JHM-D-11-048.1

Taschner, E., Folkersma, M., Martínez-Tossas, L.A., Verzijlbergh, R. & van Wingerden, J.W. (2023) A new coupling of a GPU-resident large-eddy simulation code with a multiphysics wind turbine simulation tool. *Wind Energy*, 27, 1152–1172.

Troen, I. & Mahrt, L. (1986) A simple model of the atmospheric boundary layer; sensitivity to surface evaporation. *Boundary-Layer Meteorology*, 37, 129–158.

Tung, K.K. & Orlando, W.W. (2003) The k 3 and k 5/3 energy spectrum of atmospheric turbulence: Quasigeostrophic two-level model simulation. *Journal of the Atmospheric Sciences*, 60, 824.

Verstappen, R. (2011) When does eddy viscosity damp subfilter scales sufficiently? *Journal of Scientific Computing*, 49(1), 94–110. Available from: https://doi.org/10.1007/s10915-011-9504-4

Verzijlbergh, R.A. (2021) Atmospheric flows in large wind farms. *Europhysics News*, 52, 20–23. Available from: https://doi.org/10.1051/epn/2021502

Vinnichenko, N.K. (1970) The kinetic energy spectrum in the free atmosphere-1 second to 5 years. *Tellus*, 22, 158–166. Available from: https://doi.org/10.1111/j.2153-3490.1970.tb01517.x

Volonté, A., Gray, S.L., Clark, P.A., Martínez-Alvarado, O. & Ackerley, D. (2024) Strong surface winds in storm Eunice. Part 1: storm overview and indications of sting jet activity from observations and model data. *Weather*, 79, 40–45. Available from: https://doi.org/10.1002/wea.4402

Williams, S., Dubreuil-B, C. & Seim, K.S. (2024) Multi-fidelity wake model validation at the arkona offshore wind farm. In: *Conference session at Wind Europe Technology Workshop*. Available from: https://windeurope.org/tech2024/programme/presentations/65/ Accessed 2nd October 2025.

Zanaga, D., Van De Kerchove, R., Daems, D., De Keersmaecker, W., Brockmann, C. & Kirches, G. (2022) Esa worldcover 10 m 2021 v200. https://doi.org/10.5281/zenodo.7254221

Zhou, B., Simon, J.S. & Chow, F.K. (2014) The convective boundary layer in the terra incognita. *Journal of the Atmospheric Sciences*, 71, 2545–2563. Available from: https://doi.org/10.1175/JAS-D-13-0356.1

How to cite this article: Postema, B., van Heerwaarden, C.C., van Stratum, B.J., van Dorp, P., Baas, P. & Jonker, H.J. (2026) Simulating the year to minute wind spectrum with mesoscale-coupled large-eddy simulations. *Quarterly Journal of the Royal Meteorological Society*, e70147. Available from: https://doi.org/10.1002/qj.70147